Computational Materials Science 187 (2021) 110059

Contents lists available at ScienceDirect

Computational Materials Science

journal homepage: www.elsevier.com/locate/commatsci

A Novel Method for Estimating the Charge Equilibrium within the Dendrites of Rechargeable Batteries

Asghar Aryanfar [a,b,*], Dimitri M. Saad [a], William A. Goddard III [c]

[a] American University of Beirut, Riad ElSolh, Beirut 1107-2020, Lebanon
[b] Bahçeşehir University, 4 çırağan Cad, Beşiktaş, Istanbul 34353, Turkey
[c] California Institute of Technology, 1200 E California Blvd, Pasadena, CA 91125, United States

ARTICLE INFO

Keywords:
Charge equilibrium
Dendritic microstructures
Optimization

ABSTRACT

The nonuniform formation and growth of microstructures during the electrochemical charging of a battery is the main reason for the short circuit and capacity fade. The charge distribution across the micro-structure is the result of both local and global equilibrium which is a non-convex problem merely due to random placement of the atoms. As such, obtaining the charge equilibrium (*QEq*) is critical, since the amount of withheldcharge determines the success rate of the bond formation for the ionic species approaching the microstructure which ultimately determines the morphology of the electrochemical deposits. Herein we develop a computationally-affordable method for estimating the charge allocation within such microstructures. The cost function and the span of the charge distribution correlates very closely with the trivial method as well as a conventional method, albeit having significantly less computational cost. The method can be used for optimization in non-convex problems, specially for those of randomly-formed morphology.

1. Introduction

Metallic anodes such as lithium, sodium and zinc are arguably highly attractive candidates for use in high-energy and high-power density rechargeable batteries [1–3]. In particular, lithium metal possess the lowest density and smallest ionic radius which provides a very high gravimetric energy density and possesses the highest electropositivity ($E^0 = -3.04\ V$ vs SHE) that likely provides the highest possible voltage, making it suitable for high-power applications such as electric vehicles. ($\rho = 0.53\ g.cm^{-3}$) [4,5]. During the charging, the fast-pace formation of microstructures with relatively low surface energy from Brownian dynamics, leads to the branched evolution with high surface to volume ratio [6]. The quickening tree-like morphologies could occupy a large volume, possibly reach the counter-electrode and short the cell (Fig. 1a). Additionally, they can also dissolve from their thinner necks during subsequent discharge period. Such a formation-dissolution cycle is particularly prominent for the metal electrodes due to lack of intercalation[1] [1]. Previous studies have investigated various factors on dendritic formation such as current density [7], electrode surface roughness [8–10], impurities [11], solvent and electrolyte chemical composition [12,13], electrolyte concentration [14], utilization of powder electrodes [15] and adhesive polymers [16], temperature [17], guiding scaffolds [18,19], capillary pressure [20], cathode morphology [21] and mechanics [22,23]. Some of conventional characterization techniques used include NMR [24] and MRI [25]. Recent studies also have shown the necessity of stability of solid electrolyte interphase (i.e. SEI) layer for controlling the nucleation and growth of the branched medium [26,27].

Earlier model of dendrites had focused on the electric field and space charge as the main responsible mechanism [28] while the later models focused on ionic concentration causing the diffusion limited aggregation (DLA) [29–31]. Both mechanisms are part of the electrochemical potential [32,33], indicating that each could be dominant depending on the localizations of the electric potential or ionic concentration within the medium. Nevertheless, their interplay has been explored rarely, especially in continuum scale and realistic time intervals, matching scales of the experimental time and space.

Recent works, have addressed the nucleation aspect of electrodeposition via tuning surface energy and the radius of the interface [34,35]. Dendrites instigation is rooted in the non-uniformity of electrode surface morphology at the atomic scale combined with Brownian ionic motion during electrodeposition. Any asperity in the surface provides a sharp electric field that attracts the upcoming ions as a deposition sink. Indeed

* Corresponding author.
E-mail address: aryanfar@caltech.edu (A. Aryanfar).

[1] Intercalation: diffusion into inner layer as the housing for the charge, as opposed to depositing in the surface.

https://doi.org/10.1016/j.commatsci.2020.110059
Received 4 June 2020; Received in revised form 8 September 2020; Accepted 9 September 2020
Available online 14 October 2020

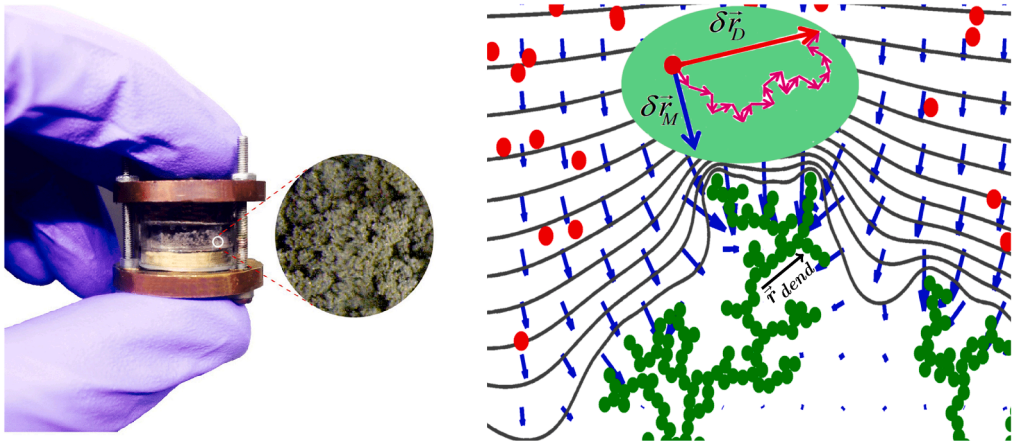

(a) Lab-scale observation of dendritic microstructures. [17]

(b) The transport elements in the coarse scale of time, representing branch vector $\vec{r}_{dend}$. [44]

Fig. 1. Observation/Modeling of dendritic propagation [36].

the closeness of a dendritic spike to the counter electrode, as the source of ionic release, is another contributing factor. In fact, the same mechanism is responsible for the further semi-exponential growth of dendrites in any scale. During each pulse period the ions accumulate at the dendrites tips (unfavorable) due to high electric field in bulging geometry and during each subsequent rest period the ions tend to diffuse away to other less concentrated regions (favorable) [36]. The relaxation of ionic concentration during the idle period provides a useful mechanism to achieve uniform deposition and growth during the subsequent pulse interval. Such dynamics typically occurs within the double layer (or stern layer [37]) which is relatively small and comparable to the Debye length. In high charge rates, the ionic concentration is depleted and concentration on the depletion reaches zero [38]; nonetheless, our continuum-level study extends to larger scale, beyond the double layer region [39].

Various charging protocols have been utilized for the prevention of dendrites [40], which has previously been used for uniform electroplating [41]. We have proven that the optimum rest period for the suppression of dendrites correlates with the relaxation time of the double layer for the blocking electrodes which is interpreted as the *RC time* of the electrochemical system [42]. We have explained qualitatively how relatively longer pulse periods with identical duty cycles will lead to longer and more quickening growing dendrites [43]. We developed coarse grained computationally affordable algorithm that allowed us reach to the experimental time scale ($\sim ms$). Additionally, in the recent theoretical work we indicated that there is an analytical criterion for the optimal inhibition of growing dendrites [44].

Additionally, the ultimate morphology of the dendritic electrodeposits, depends on the possibility of the bond-formation when ion reaches the outer boundary of the microstructure. The success of electron transfer in such approach would highly be determined to the amount of the charge presents in the electron transfer site. Therefore, in this paper, we elaborate on the charge distribution in equilibrium across the dendritic microstructures, where the placement of the stochastically-grown dendrites. Subsequently, we verify our method via comparison with trivial method, which is far more computationally expensive as well as a conventional package. This affordable method of computation for charge distribution can be utilized for any given microstructure, specially those of large scales.

2. Methodology

2.1. Computational method

Fig. 1 represents the dendritic evolution in the lab scale as well as in our computations. The ionic flux is generated in response to the variation of the electrochemical potential, which is per see the result of the variations (i.e. gradient) of concentration (∇C) or electric potential (∇V). In the ionic scale, the regions of higher concentration tend to collide and repel more and, given enough time, diffuse to lower concentration zones, following Brownian motion. Such inter-collisions could be added-up in the larger scale and be addressed via diffusion length [43] [2] representing the average progress of a diffusive wave in a given time and is obtained directly from the diffusion equation [46]. On the other hand, ions tend to acquire drift velocity in the electrolyte medium when exposed to electric field and during the given time δt their progress by the drift velocity.

Therefore the total effective displacement $\delta\vec{\mathbf{r}}$ with neglecting convection[3] would be:

$$\vec{\mathbf{r}}(t+\delta t) = \vec{\mathbf{r}}(t) + \sqrt{2D^{+}\delta t}\,\hat{\mathbf{g}} + \mu^{+}\vec{\mathbf{E}}\delta t \tag{1}$$

where D^{+} is the ionic diffusion coefficient in the electrolyte, δt is the coarse time interval,[4] $\hat{\mathbf{g}}$ is a normalized vector in random direction, representing the Brownian dynamics, μ^{+} is the mobility of cations in electrolyte and $\vec{\mathbf{E}}$ is the local electric field, which is the gradient of electric potential ($\vec{\mathbf{E}} = -\nabla V$). Such vector sum is represented in the Fig. 1b.

The probability of successful jump depends on how much charge each atom has from the sea of electrons. Such charge equilibrium would be obtained from the minimization of the total potential energy for the amorphous material, which is generally obtained by means of Taylor expansion as [48]:

$$E_A(Q) = E_{A0} + Q_A\left(\frac{\partial E}{\partial Q}\right)_{A0} + \frac{1}{2}Q_A^2\left(\frac{\partial^2 E}{\partial Q^2}\right)_{A0} + \cdots \tag{2}$$

where the second term in Eq. (2) is in fact the electronegativity χ and is defined by:

$$\chi_A = \frac{\partial E}{\partial Q_A}$$

[2] The diffusion coefficient D^{+} is generally concentration dependent [45], due to dilute concentration in the electro-neutral region, we assume the negligible variations.

[3] Convection-wise, since the Rayleigh number Ra is highly dependent to the thickness (i.e. $Ra \propto l^3$), for a thin layer of electrodeposition we have $Ra < 1500$ and thus the convection is negligible [47].

[4] $\delta t = \sum_{i=1}^{n}\delta t_i$ where δt_k is the inter-collision time, typically in the range of fs.

since all the composing atoms in dendrites are identical the variation in fact breaks down to the cost function as the *difference* in the total potential energy $E(Q)$ based on the charge allocation as:

$$E(Q) = \sum_{i=1}^{n} \sum_{j=i+1}^{n} \frac{q_i q_j}{d_{i,j}} \tag{3}$$

where d_{ij} is the interatomic distance from i to j defined as:

$$d_{i,j} = |\vec{r}_j - \vec{r}_i|$$

and $\vec{r}_i$ and $\vec{r}_j$ are the coordinates of the atoms relative to a reference point. Assuming that the set of charge values could be represented by the vector $q = [\, q_1 \quad \dots \quad q_n \,]$, one can interpret the optimization problem in the quadratic form as:

$$\text{minimize} \frac{1}{2} q^T R q$$

$$\text{s.t.} \quad \begin{cases} \sum_{i=1}^{n} q_i = Q \\ 0 \leqslant q_i \leqslant ne \end{cases} \tag{4}$$

where the total energy is in fact the matrix from of Eq. (3) and the reciprocal distance matrix R is stablished:

$$R = \begin{bmatrix} 0 & \frac{1}{d_{1,2}} & \cdots & \frac{1}{d_{1,n}} \\ \frac{1}{d_{2,1}} & \ddots & & \vdots \\ \vdots & & \ddots & \\ \frac{1}{d_{n,1}} & \cdots & & 0 \end{bmatrix}$$

and n and e are the valence electrons and electron charge respectively. The first constraint in Eq. (4) means that the total sum of charges is a constant value Q given to the dendrite and the second and third constraints determine the capacity range of charge fraction for each atom in the microstructure.

2.1.1. Locating minimum charge

The energy difference defined by Eq. (4) as the cost function is depends on the charge allocation in the atoms as well as their distance. Assuming the given charge q_i to a charge, in order to minimize the energy term $\frac{q_i q_j}{2d_{i,j}}$, the corresponding charges q_j with the lower distance (closer) should contain lower relative charge values and vice versa. In fact the allocation of charges should be such that the most populated atomic regions in the crystal, formed by the random walk procedure, should contain the lowest fraction of the charge, since the denominator in the Eq. (3) is quite large in those regions. Such position in fact could be obtained for the case of even distribution in the atomic charges. Assuming q_{min} as such position, the value of the reciprocal distance sum $\frac{1}{d_{min,k}}$ should be the maximum:

$$\max_{k} \sum_{i=1}^{n-1} \frac{1}{d_{min,k}} \tag{5}$$

The minimum charge q_{min} via this expression signifies it's the closest proximity to the other charges.

2.1.2. Charge distribution

Finding the closest proximity of the minimum charge q_{min} in the Eq. (5) ensures the closest radial distance to the surrounding atoms. In other words, the largest allocation of charge magnitude should be given to the atoms farthest from the most compact regions. Therefore, starting from the minimum charge q_{min} as the reference and moving outward radially, any charge distribution should have an increasing trend, and there will be no sensitivity for variation in the azimuthal direction as:

$$\frac{\delta q}{\delta \theta} = 0$$

As well, the quadratic form of the potential energy $E(Q)$ in Eq. (3) suggests that the charge distribution in the radial direction has rounded-up geometry, which we translate in the radial direction r to:

$$\frac{\delta^2 q}{\delta r^2} \geqslant 0$$

Performing numerical segmentation, this typically leads to $q_{i+1} - 2q_i + q_{i-1} \geq 0$ for consecutive charges. Since the atoms possess non-uniform spacing, we arrive at:

$$\frac{\frac{\delta q_{k+1}}{\delta r} - \frac{\delta q_k}{\delta r}}{d_{k+1,k-1}} \geqslant 0$$

noting the difference in the slope m we arrive the following:

$$\frac{q_{k+1} - q_k}{d_{k+1,k}} - \frac{q_k - q_{k-1}}{d_{k,k-1}} = m$$

therefore the value of charge q_{k+1} consecutively can be obtained as:

$$q_{k+1} = q_k + \frac{d_{k+1,k}}{d_{k,k-1}} (q_k - q_{k-1}) + m d_{k+1,k} \tag{6}$$

The Eq. (6) assigns a charge value to atom $k+1$ based on charge values of the 2 preceding atoms $k-1$ and k, starting from the minimum charge located in the previous section. Such iteration has been performed for multiple values of the variation difference m for the charge distribution based on the constraints in the Eq. (4) such that the minimum value of the objective function (Eq. 3) is obtained. The outlined algorithm has been visualized in the Fig. 2 based on the parameters given in the Table 1. Fig. 3 shows the charge distribution within the given stochastically-developed microstructure, where the location of the minimum charge is highlighted. The black lines and green vectors represent the iso-potential contours and electric field respectively.

2.2. Sample computation

We carry out the sample computation for the method we have developed and we compare it against the conventional MATLAB framework, as well as the trivial solutions, and filtered trivial solution. We study the one dimensional case where atoms are allocated in a straight line based on the numbers given in the Table 2. Here we propose the following methods to compare to:

2.2.1. Analytical solution

Since the central position from Eq. (3) can be regarded as the minimum charge point, we can interpret that the center of the 1D line could be the location for the minimum charge. From the constraints in the Eq. (4), the type of analytical function can be extracted. The charge should have the increasing slope condition as well as positive second derivative for the formation of the rounded-up shape. If x is the one dimensional coordinates, therefore analogous to the given constraints the forms are obtained as:

$$\begin{cases} \frac{\partial \rho}{\partial x} \geqslant 0 & \sim \alpha x \\ \frac{\partial^2 \rho}{\partial x^2} \geqslant 0 & \sim \beta \exp(x) \end{cases}$$

where $\{\alpha, \beta\} > 0$. The line will have a symmetric charge distribution, one could study one of it's identical halves, using the combinatorics the two forms via absorbing the two coefficients α and β into the new prefactor a. Considering the continuum-scale linear charge density $\rho(x)$

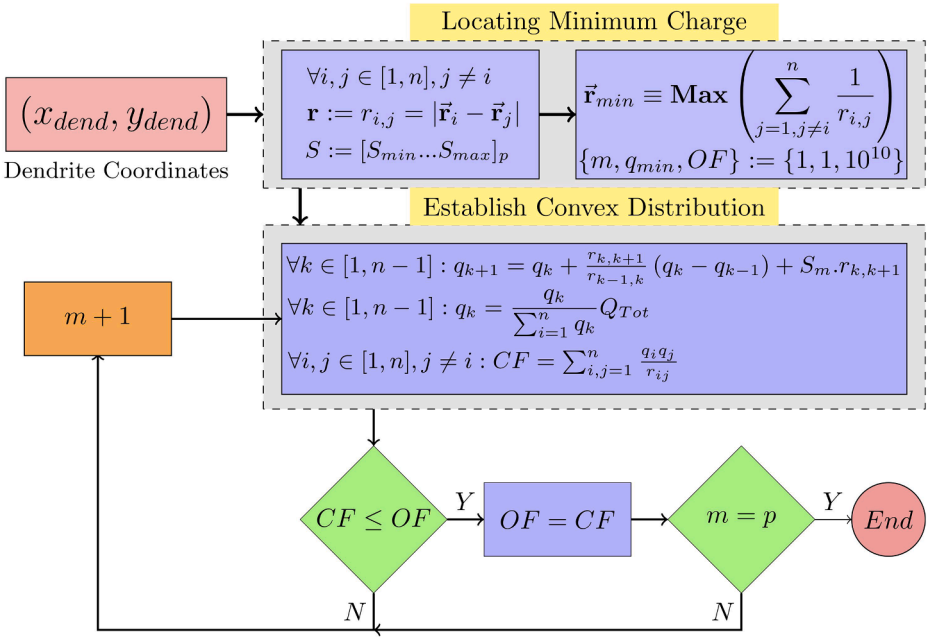

Fig. 2. The charge-equilibrium pseudo-code.

Table 1
Parameters for sample computation [43].

Parameter	Symbol	Value	Unit
# atoms	n	300	[]
Diffusivity	D^+	1.4×10^{-14}	$m^2.s^{-1}$
Permittivity	ε	64	[]
Temperature	T	293	K
Domain length	l	180	nm
Voltage	ΔV	0.1	V

the charge distribution would have a form of:

$$\rho(x) = ax\exp(bx)$$

Therefore the energy minimization in Eq. (4) will translate into the following:

$$\text{minimize} \int_0^l \frac{\rho(x)}{x} dx$$

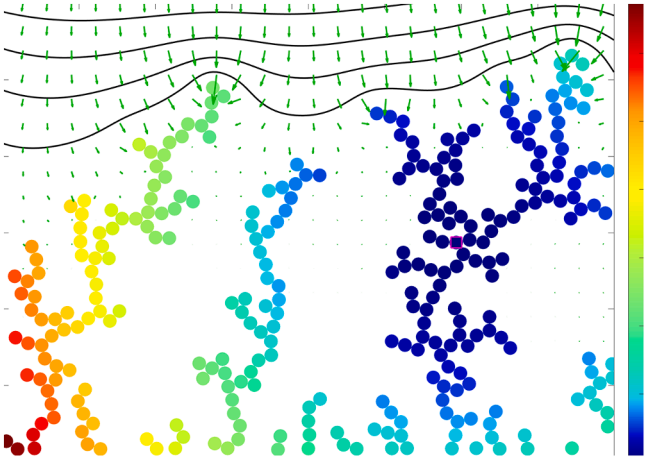

Fig. 3. Dimension-less Charge distribution across the microstructure. The minimum charge is illustrated with square.

$$\text{s.t.} \begin{cases} \int_0^l \rho(x)dx = Q \\ 0 \leqslant \rho(x) \leqslant ne \end{cases} \quad (7)$$

2.2.2. Exact solution

Assuming: $\rho = axe^{bx}$, one needs to find two free parameters a, b. The total energy $E(Q)$ can be obtained as:

$$E(Q) = \frac{a}{b}(\exp(bl) - 1)$$

and the constraints will be obtained using the chain derivative rule as:

$$Q = \int_0^l axe\exp(bx)dx = \frac{a}{b}x\exp(bx)|_0^l - \int_0^l \frac{a}{b}\exp(bx) = \left(\frac{al}{b}e^{bl} - \frac{a}{b^2}(e^{bl} - 1)\right)$$

Since the distribution form $\rho(x)$ is increasing the boundary condition should satisfy at the end ($x = l$) and therefore:

$$\begin{cases} \frac{a}{b}\left(le^{bl} - \frac{1}{b}e^{bl} - \frac{1}{b}\right) = Q \\ ale^{bl} \leqslant := 1 \\ a \geqslant 0 \end{cases}$$

Considering the maximum value in the inequality, we arrive to the following via combination:

$$\left(\frac{1}{b} - \frac{1}{abl} - \frac{a}{b^2}\right) = Q$$

This is a quadratic equation versus the exponent b. Therefore, assuming $a = 1$ it can be solved and the charge density is obtained as:

Table 2
Verification parameters.

Q	n	x_{min}	x_{max}	q_{min}	q_{max}
11	11	−10	10	0	3.66

$$\rho(x) = x\exp\left(\left(\frac{l-1\pm\sqrt{(l-1)^2-4Ql}}{2Ql}\right)x\right) \tag{8}$$

2.2.3. Simplified solution

The exact form of charge distribution in Eq. (8) can be approximated with a simpler form. Here we prove that the exponent has an upper bound of $\frac{1}{l}$:

$$\frac{l-1\pm\sqrt{(l-1)^2-4Ql}}{2Ql}\leqslant\frac{1}{l}$$

Proving for maximum case one has:

$$\sqrt{(l-1)^2-4Ql}\leqslant(1-l)+2Q \tag{9}$$

Since the *LHS* is positive value, the *RHS* we must have:

$$l\leq 2Q+1$$

As well the square sign should be non-negative, therefore:

$$(l-1)^2-4Ql\geqslant 0$$

$$l\leq 2Q+1-2\sqrt{Q(Q+1)}$$

Taking the inequality (9) to the power 2 we get:

$$0\leqslant Q(Q+1)\checkmark$$

which is always true and the upper bound is determined. Therefore the exponent could be considered as $b:=\frac{1}{l}$. Thus the sum condition gives:

$$Q=\int_0^l axe^{\frac{x}{l}}=\left(alxe^{\frac{x}{l}}-\int_0^l ale^{\frac{x}{l}}\right)\Bigg|_0^l=al^2$$

and the coefficient a is updated accordingly versus the total charge sum Q. Hence, the simplified charge would be:

$$\rho(x)=\frac{Q}{l^2}xe^{\frac{x}{l}} \tag{10}$$

Note that this is valid for $x\geqslant 0$ and the other (negative) half can be established from symmetry.

2.2.4. Enhanced trivial method

Using the trivial method, we iteratively scan the charge distribution $\{q_1,\ldots,q_n\}$ which minimizes the total energy $E(Q)$ in Eq. (4) from the all possible permutations from combinatorics. The approximate iterative solution could be finding the non-zero integer distribution to the pre-determined sum constraint Q given as:

$$q_1+\cdots+q_n=pQ \tag{11}$$

where, due to integer nature of the solution, the fixed total sum has been augmented p-fold to allow higher precision of the distribution and the resulted distribution will ultimately scaled back p-fold to satisfy the sum constraint in Eq. (4). As well, the range constraints could been translated into the followings to save a significant portion of the trivial solutions from Eq. (11):

$$\begin{cases} q_{k+1}\geqslant q_k \\ q_{k+1}-2q_k+q_{k-1}\geqslant 0 \end{cases} \tag{12}$$

The next comparison has been performed with the conventional MATLAB package function *fmincon* in terms of cost and accuracy. Since this function locates the local minima, it was run for 5 different initial distribution values in the close proximity of the analytical solution, to target the global minimum. As well, the initial condition was given based on the analytical solution in the Eq. (10).

The resulted distributions have been visualized in the Fig. 4a and the corresponding significant numbers are compared in the Fig. 4a. It is worth noting that the computational time required for the trivial case post-filtration is significantly less than the filtered cases via Eq. (12), with the factor of $\sim 10^5$.

3. Results & discussions

Finding the minimum energy $E(Q)$ for randomly-formedmicrostructures is usually a non-convex problem, which makes it difficult to solve. This is merely due to stochastic allocation of the atoms. Since the reciprocal distance matrix R is symmetric ($R_{i,j}=R_{j,i}$), for any given matrix B there exists matrix Z such that:

$$R=B^{-1}ZB$$

Due to symmetry, the trace of reciprocal matrix $tr(R)$ is the sum of it's eigenvalues λ_i. Since, the distance of each atom to itself is zero, $tr(R)=0$ and hence:

$$tr(R)=\sum\lambda_i=diag(R)=0$$

the zero-sum constraint shows that at least one eigenvalue is negative. Therefore the problem is not convex.

The flowchart 2 shows the information flow for determining the charge allocation leading to the minimum energy $E(Q)$, which is mainly divided into two compartment of *locating the minimum charge*, and *establishing acurved-upcharge distribution*. Such division in fact is an approximation, providing a significantly less computational cost versus the *whole-in*minimization of the total energy $E(Q)$ given in the Eq. (3). In fact, the minimization of the reciprocal distance sum in the Eq. (5) ensures that the most populated central (body) regions would be the location of the minimum charge and vice versa, the outer (boundary) regions would possess the highest portion of the charge sum, since they will be farthest from the rest of the atoms to create large potentials. This has been illustrated in the random dendritic microstructure illustrated in the Fig. 3. Such allocation means that the outer atoms in fact will have higher possibility for the electron donation rather than the inner layers.

The comparative analysis of our method has been performed for the 1D arrangement of the atoms based on the Table 2. The verification has been illustrated versus the enhanced trivial search method as well as the commercial package. The accuracy comparison is shown in the Fig. 4a and the effectiveness is represented in the Fig. 4b.

Additionally the advantage of the developed method is that the result is independent of the initial condition, as opposed to the commercial package. Typical methods of finding the optimum solution requires wither restricting the search within a convex set [49], or relaxing non-convex constraints [50,51]. Our method is numerically following the same track, searching iteratively via small perturbations in the roundedness (Fig. 5a) to obtain the minimum energy $E(Q)$. Additionally the developed method finds the optimum charge distribution via the physical and spatial awareness of the curved-up dispersal of the charge. Such convex hull is illustrated in the Fig. 5b, where the colors qualitatively represent the relative charge values.

Ultimately, the role of the peaks in the boundary of the microstructure for accumulating charge relative to the inner and flat regions lies in it's geometry (i.e. radius). The sharp boundary determines competitiveness of the two neighboring zones over a physical parameter. This is analogous to the build-up of stress ΔP in the nucleation of microstructure via the following relationship [34]:

$$\Delta P=\gamma\left(\frac{1}{R_1}+\frac{1}{R_2}\right)$$

where γ is the corresponding surface energy and R_1 and R_2 are the respective radius of curvature in a given orthogonal directions. The sharp interface, therefore is meta-stable and possess higher energy, which is known as Kelvin effect [52].

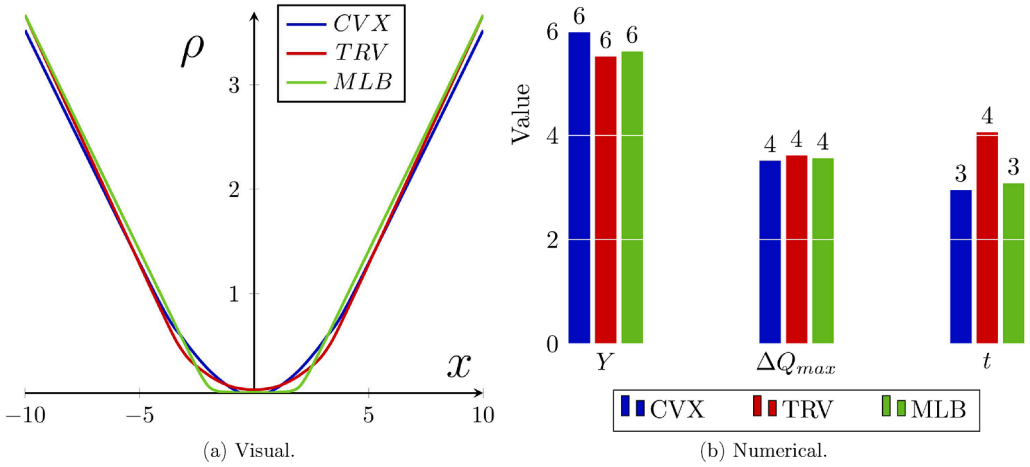

(a) Visual. (b) Numerical.

Fig. 4. Comparison.

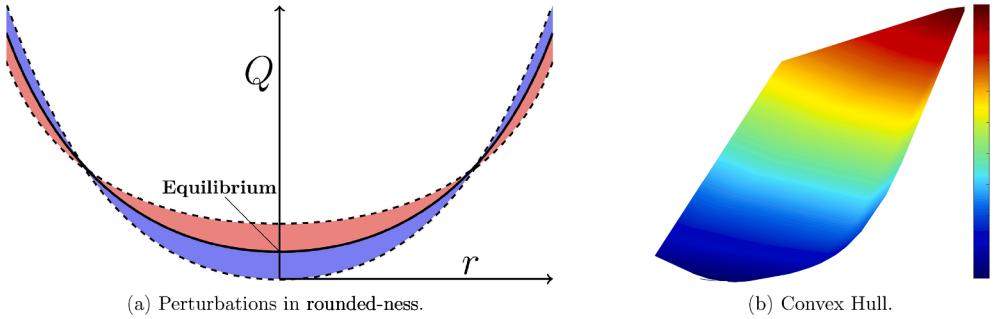

(a) Perturbations in rounded-ness. (b) Convex Hull.

Fig. 5. Analysis.

4. Conclusions

In this paper, we developed a computational method for determining charge equilibrium distributionwithin the given stochastically-evolved dendritic microstructure. Our computationally affordable method, which has mainly been divided to simpler compartments, has been compared against the conventional method as well as the commercial package.

The significance of this method is the independence from the initial condition and very low computational cost. Our method could be used for determining the charge allocation in a larger-than-conventional clusters of microstructures where the convex optimization is not feasible. the charge magnitude would determine the reaction probability, the rate of propagation and the densification of microstructure during the branched evolution.

CRediT authorship contribution statement

Asghar Aryanfar: Conceptualization, Validation, Formal analysis, Investigation, Data curation, Writing - original draft, Writing - review & editing, Visualization, Funding acquisition. **Dimitri M. Saad:** Methodology, Resources, Software, Writing - review & editing, Supervision, Project administration. **William A. Goddard III:** Supervision, Project administration.

Declaration of Competing Interest

The authors declare that they have no known competing financial interests or personal relationships that could have appeared to influence the work reported in this paper.

Acknowledgement

The authors would like to thank internal support from the Faculty of Engineering and Architecture at American University of Beirut.

Appendix A. Supplementary data

Supplementary data associated with this article can be found, in the online version, athttps://doi.org/10.1016/j.commatsci.2020.110059.

References

[1] Zhe Li, Jun Huang, Bor Yann Liaw, Viktor Metzler, Jianbo Zhang. A review of lithium deposition in lithium-ion and lithium metal secondary batteries, Journal of Power Sources 254 (2014) 168–182.
[2] Pucheng Pei, Keliang Wang, Ze Ma, Technologies for extending zinc air batterys cyclelife: A review, Applied Energy 128 (2014) 315–324.
[3] Michael D Slater, Donghan Kim, Eungje Lee, Christopher S Johnson, Sodium-ion batteries, Advanced Functional Materials 23 (8) (2013) 947–958.
[4] Siyuan Li, Jixiang Yang, Yingying Lu. Lithium metal anode, Encyclopedia of Inorganic and Bioinorganic Chemistry 1–21.
[5] W. Xu, J.L. Wang, F. Ding, X.L. Chen, E. Nasybutin, Y.H. Zhang, J.G. Zhang, Lithium metal anodes for rechargeable batteries, Energy and Environmental Science 7 (2) (2014) 513–537.
[6] Xu. Kang, Nonaqueous liquid electrolytes for lithium-based rechargeable batteries, Chemical Reviews-Columbus 104 (10) (2004) 4303–4418.
[7] F. Orsini, A.D. Pasquier, B. Beaudoin, J.M. Tarascon, et al., In situ scanning electron microscopy (sem) observation of interfaces with plastic lithium batteries, Journal Power Sources 76 (1998) 19–29.
[8] C. Monroe, J. Newman, The effect of interfacial deformation on electrodeposition kinetics, Journal of the Electrochemical Society 151 (6) (2004) A880–A886.
[9] Christoffer P. Nielsen, Henrik Bruus, Morphological instability during steady electrodeposition at overlimiting currents. arXiv preprint arXiv:1505.07571, 2015.
[10] P.P. Natsiavas, K. Weinberg, D. Rosato, M. Ortiz, Effect of prestress on the stability of electrode–electrolyte interfaces during charging in lithium batteries, Journal of the Mechanics and Physics of Solids 95 (2016) 92–111.

[11] J. Steiger, D. Kramer, R. Monig, Mechanisms of dendritic growth investigated by in situ light microscopy during electrodeposition and dissolution of lithium, Journal of Power Sources 261 (2014) 112–119.

[12] N. Schweikert, A. Hofmann, M. Schulz, M. Scheuermann, S.T. Boles, T. Hanemann, H. Hahn, S. Indris, Suppressed lithium dendrite growth in lithium batteries using ionic liquid electrolytes: Investigation by electrochemical impedance spectroscopy, scanning electron microscopy, and in situ li-7 nuclear magnetic resonance spectroscopy, Journal of Power Sources 228 (2013) 237–243.

[13] Reza Younesi, Gabriel M Veith, Patrik Johansson, Kristina Edström, Tejs Vegge, Lithium salts for advanced lithium batteries: Li-metal, li-o 2, and li-s, Energy and Environmental Science 8 (7) (2015) 1905–1922.

[14] C. Brissot, M. Rosso, J.N. Chazalviel, S. Lascaud, In situ concentration cartography in the neighborhood of dendrites growing in lithium/polymer-electrolyte/lithium cells, Journal of the Electrochemical Society 146 (12) (1999) 4393–4400.

[15] I.W. Seong, C.H. Hong, B.K. Kim, W.Y. Yoon, The effects of current density and amount of discharge on dendrite formation in the lithium powder anode electrode, Journal of Power Sources 178 (2) (2008) 769–773.

[16] G.M. Stone, S.A. Mullin, A.A. Teran, D.T. Hallinan, A.M. Minor, A. Hexemer, N. P. Balsara, Resolution of the modulus versus adhesion dilemma in solid polymer electrolytes for rechargeable lithium metal batteries, Journal of the Electrochemical Society 159 (3) (2012) A222–A227.

[17] Asghar Aryanfar, Tao Cheng, Agustin J Colussi, Boris V Merinov, William A Goddard III, Michael R Hoffmann, Annealing kinetics of electrodeposited lithium dendrites, The Journal of chemical physics 143 (13) (2015), 134701.

[18] Yuanzhou Yao, Xiaohui Zhao, Amir A. Razzaq, Yuting Gu, Xietao Yuan, Rahim Shah, Yuebin Lian, Jinxuan Lei, Qiaoqiao Mu, Yong Ma, et al., Mosaic rgo layer on lithium metal anodes for effective mediation of lithium plating and stripping, Journal of Materials Chemistry A (2019).

[19] Ji Qian, Yu Li, Menglu Zhang, Rui Luo, Fujie Wang, Yusheng Ye, Yi Xing, Wanlong Li, Wenjie Qu, Lili Wang, et al., Protecting lithium/sodium metal anode with metal-organic framework based compact and robust shield, Nano Energy (2019).

[20] Wei Deng, Wenhua Zhu, Xufeng Zhou, Fei Zhao, Zhaoping Liu, Regulating capillary pressure to achieve ultralow areal mass loading metallic lithium anodes, Energy Storage Materials (2019).

[21] Alexander W Abboud, Eric J Dufek, Boryann Liaw, Implications of local current density variations on lithium plating affected by cathode particle size, Journal of The Electrochemical Society 166 (4) (2019) A667–A669.

[22] Xu. Chen, Zeeshan Ahmad, Asghar Aryanfar, Venkatasubramanian Viswanathan, Julia R Greer, Enhanced strength and temperature dependence of mechanical properties of li at small scales and its implications for li metal anodes, Proceedings of the National Academy of Sciences 114 (1) (2017) 57–61.

[23] Peng Wang, Wenjie Qu, Wei-Li Song, Haosen Chen, Renjie Chen, Daining Fang, Electro–chemo–mechanical issues at the interfaces in solid-state lithium metal batteries, Advanced Functional Materials (2019) 1900950.

[24] Rangeet Bhattacharyya, Baris Key, Hailong Chen, Adam S. Best, Anthony F. Hollenkamp, Clare P. Grey, In situ nmr observation of the formation of metallic lithium microstructures in lithium batteries, Nature Materials 9(6):504 (2010).

[25] S. Chandrashekar, Nicole M Trease, Hee Jung Chang, Du. Lin-Shu, Clare P Grey, Alexej Jerschow, 7li mri of li batteries reveals location of microstructural lithium, Nature Materials 11 (4) (2012) 311–315.

[26] Energy & Environmental Science (2019).

[27] Laleh Majari Kasmaee, Asghar Aryanfar, Zarui Chikneyan, Michael R. Hoffmann, Agustín J. Colussi, Lithium batteries: Improving solid-electrolyte interphases via underpotential solvent electropolymerization, Chemical Physics Letters 661 (2016) 65–69.

[28] J.N. Chazalviel, Electrochemical aspects of the generation of ramified metallic electrodeposits, Physical Review A 42 (12) (1990) 7355–7367.

[29] C. Monroe, J. Newman, Dendrite growth in lithium/polymer systems - a propagation model for liquid electrolytes under galvanostatic conditions, Journal of Electrochemical Society 150 (10) (2003) A1377–A1384.

[30] Thomas A. Witten, Leonard M. Sander, Diffusion-limited aggregation, Physical Review B 27(9):5686 (9) (1983) 5686.

[31] Q. Xin Zhang, Jane Wang, Katharine L. Harrison, Katherine Jungjohann, Brad L. Boyce, Scott A. Roberts, Peter M. Attia, Stephen J. Harris, Rethinking how external pressure can suppress dendrites in lithium metal batteries, Journal of The Electrochemical Society 166 (15) (2019) A3639–A3652.

[32] Allen J. Bard, Larry R. Faulkner, Electrochemical Methods: Fundamentals and Applications, Wiley, New York, 1980, 1980..

[33] Deepti Tewari, Partha P. Mukherjee, Mechanistic understanding of electrochemical plating and stripping of metal electrodes, Journal of Materials Chemistry A 7 (9) (2019) 4668–4688.

[34] Dong Wang, Wei Zhang, Weitao Zheng, Xiaoqiang Cui, Teófilo Rojo, Qiang Zhang, Towards high-safe lithium metal anodes: suppressing lithium dendrites via tuning surface energy, Advanced Science 4 (1) (2017), 1600168.

[35] Aniruddha Jana, R. Edwin Garcia, Lithium dendrite growth mechanisms in liquid electrolytes, Nano Energy 41 (2017) 552–565.

[36] Asghar Aryanfar, Michael R. Hoffmann, William A. Goddard III, Finite-pulse waves for efficient suppression of evolving mesoscale dendrites in rechargeable batteries, Physical Review E 100 (4) (2019), 042801.

[37] Martin Z Bazant, Brian D Storey, Alexei A Kornyshev, Double layer in ionic liquids: Overscreening versus crowding, Physical Review Letter 106 (4) (2011), 046102.

[38] V. Fleury, Branched fractal patterns in non-equilibrium electrochemical deposition from oscillatory nucleation and growth, Nature 390 (6656) (1997) 145–148.

[39] Asghar Aryanfar, Daniel J. Brooks, Agustín J. Colussi, Boris V. Merinov, William A. Goddard III, Michael R. Hoffmann, Thermal relaxation of lithium dendrites, Physical Chemistry Chemical Physics 17 (12) (2015) 8000–8005.

[40] Jun Li, Edward Murphy, Jack Winnick, Paul A Kohl, The effects of pulse charging on cycling characteristics of commercial lithium-ion batteries, Journal of Power Sources 102 (1) (2001) 302–309.

[41] M.S. Chandrasekar, M. Pushpavanam, Pulse and pulse reverse plating – conceptual, advantages and applications, Electrochimica Acta 53 (8) (2008) 3313–3322.

[42] M.Z. Bazant, K. Thornton, A. Ajdari, Diffuse-charge dynamics in electrochemical systems, Physical Review E 70 (2) (2004).

[43] Asghar Aryanfar, Daniel Brooks, Boris V. Merinov, William A. Goddard Iii, Agustín J. Colussi, Michael R. Hoffmann. Dynamics of lithium dendrite growth and inhibition: Pulse charging experiments and monte carlo calculations, The Journal of Physical Chemistry Letters 5(10) (2014) 1721–1726.

[44] Asghar Aryanfar, Daniel J. Brooks, William A. Goddard, Theoretical pulse charge for the optimal inhibition of growing dendrites, MRS Advances 3 (22) (2018) 1201–1207.

[45] S. Chandrashekar, Onyekachi Oparaji, Guang Yang, Daniel Hallinan, Communication 7li mri unveils concentration dependent diffusion in polymer electrolyte batteries, Journal of The Electrochemical Society 163 (14) (2016) A2988–A2990.

[46] Jean Philibert, One and a half century of diffusion: Fick, einstein, before and beyond, Diffusion Fundamentals 4 (6) (2006) 1–19.

[47] Philip J. Pritchard, John W. Mitchell, John C. Leylegian, Fox and McDonald's Introduction to Fluid Mechanics, Binder Ready Version, John Wiley & Sons (2016).

[48] Anthony K. Rappe, William A. Goddard III, Charge equilibration for molecular dynamics simulations, The Journal of Physical Chemistry 95 (8) (1991) 3358–3363.

[49] Behçet Açıkmeşe, John M Carson, Lars Blackmore, Lossless convexification of nonconvex control bound and pointing constraints of the soft landing optimal control problem, IEEE Transactions on Control Systems Technology 21 (6) (2013) 2104–2113.

[50] Changliu Liu, Chung-Yen Lin, Yizhou Wang, Masayoshi Tomizuka, Convex feasible set algorithm for constrained trajectory smoothing, in: 2017 American Control Conference (ACC), IEEE, 2017, pp. 4177–4182.

[51] Changliu Liu, Chung-Yen Lin, Masayoshi Tomizuka, The convex feasible set algorithm for real time optimization in motion planning, SIAM Journal on Control and Optimization 56 (4) (2018) 2712–2733.

[52] Asghar Aryanfar, Daniel J. Brooks, Agustin J. Colussi, Michael R. Hoffmann, Quantifying the dependence of dead lithium losses on the cycling period in lithium metal batteries, Physical Chemistry Chemical Physics 16 (45) (2014) 24965–24970.